Research Article

Azzeddine Belaziz* and Mohamed Mazari

Experimental and Numerical Study of Bead Welding Behavior of HDPE Pipe Under Uniaxial Loading

https://doi.org/10.2478/mme-2019-0024
Received Jan 23, 2018; revised Sep 1, 2018; accepted Nov 20, 2018

Abstract: The present paper is devoted to the experimental study of the mechanical behavior of high-density polyethylene structure subjected to traction and welded by means of butt-welding process. We were based ourselves on experimental tests which have been carried out to characterize the material studied, introducing the ductility or fragility of the bead welded section, and understood the effect of crosshead speeds on the mechanical behavior of the weld bead. The experimental results of the welded specimens are compared with those corresponding to the base material. In this study, two crosshead speeds of 10 and 50 mm/min were applied to make the comparison.

Keywords: High-density polyethylene (HDPE), Uniaxial tensile, Mechanical behavior, Fusion temperature

1 Introduction

Butt-welding is adopted as a process of assembling high-density polyethylene (HDPE) pipes of different diameters (Di) to transport gas or water and this depends on the welding conditions.

Various authors such as Costa *et al.* [1] have studied and proposed the classification of fusion consolidation of thermoplastic matrix composites and several studies have been carried out to study the simulation of large deformations in polymers.

Neale and Tugcu [2] carried out an FEM analysis of a cylindrical tensile test specimen and studied the deformation in HDPE thoroughly at the microscopic and macroscopic levels.

Zhang and Ben Jar [3] used a phenomenological hybrid approach based on experimental tests and FE simulations to model the deformation and ductile fracture of annular samples prepared from a commercial polymer tube and studied the effect of the rate of change of damage on the deformation and rupture behavior of a sample of polymer pipe.

The main aim of this study is to compare and estimate the durability between two cases, unwelded and welded specimens of HDPE, by means of butt fusion procedure to know the physical quantities and understanding the effect of the deformation velocity on the mechanical behavior of the weld joint (bead) of a HDPE pipe welded by conditions proposed by us, such as the melting temperature and the pressure force, as defined in Table 1.

We performed two trials for each case and for the same stretching rates (V_e). The temperature of all the tests equals the ambient temperature (T_a = 23°C); the ratio of the nominal dimensions, SDR, of the tubes (diameter and thickness) is constant. This constant is determined using Equation (1):

$$SDR = \frac{D_e}{e} \tag{1}$$

2 Experimental study

2.1 Material studied

The material used in this study is HDPE. It is a semicrystalline thermoplastic widely used in engineering applications such as pipelines and pressure vessels. In the literature, various studies [4–6] have examined the microscopic structure and plastic deformation processes of thin films of HDPE. Figure 1 shows the observation of the formation of microstructural defects by SEM in HDPE [7]. The study ma-

***Corresponding Author: Azzeddine Belaziz:** Laboratory of Materials and Reactive Systems (LMSR), Mechanical Engineering Department, Faculty of Technology, University of Sidi Bel Abbes, Algeria; Email: belaziz_azze@yahoo.com
Mohamed Mazari: Laboratory of Materials and Reactive Systems (LMSR), Mechanical Engineering Department, Faculty of Technology, University of Sidi Bel Abbes, Algeria; Email: mazari_m@yahoo.fr

Table 1: Butt-Welding Parameters

Article		PN		Thickness (mm)		Temperature (°C)
De = 315 mm		PN 16		28.2 × 29.2		203
Process 1		Process 2		Process 3		SDR
Bar	||	Bar	Sec	Bar	Min	
66	3	9	286	66	35	11

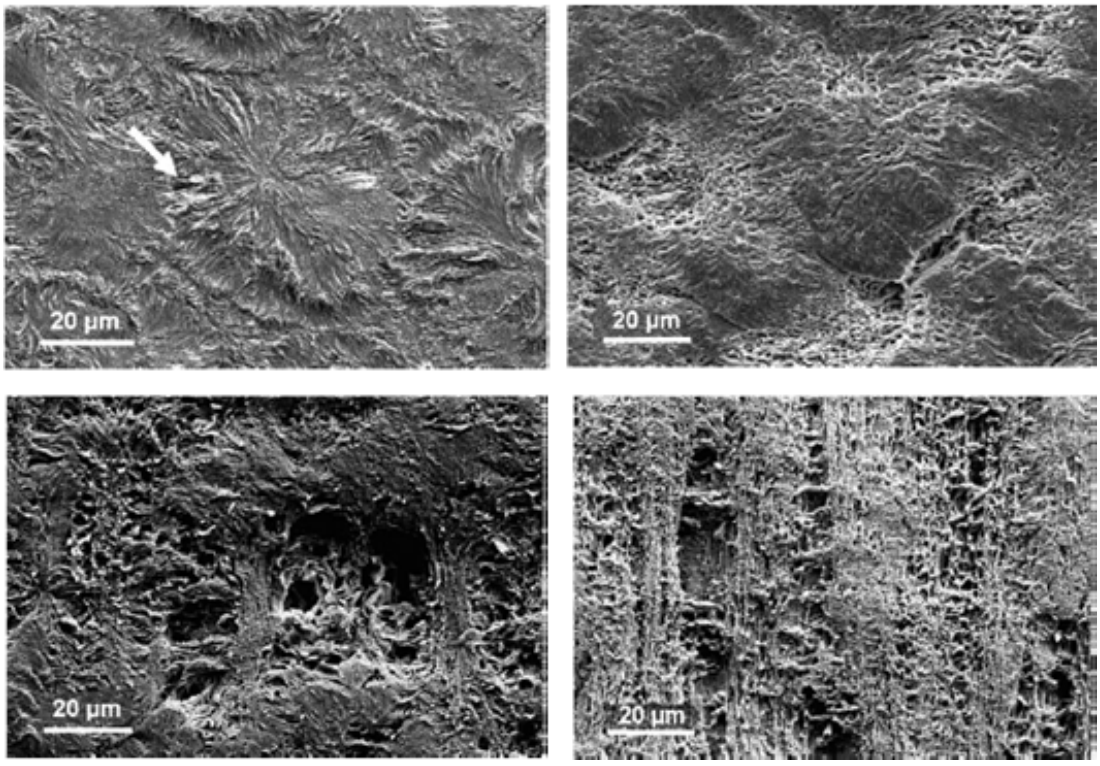

Figure 1: Observation of the formation of microstructural defects by SEM in HDPE [7]

terial was manufactured as granules and imported by the company STPM CHIALI located in Sidi Bel Abbes (Algeria) [8]. It was then extruded to make tubes of different diameters. The extrusion conditions are determined in order to ensure the most homogeneous cooling.

The technical, physical, and chemical specifications of the material studied are summarized in Table 2.

Table 2: Characteristics of HDPE Studied

Density	930 kg/m^3
Molecular weight (Mw)	310,000 (g/mole)
Crystallinity rate (Xc)	74%
Fusion temperature (T_f)	203°C
Fluidity index	0.2–1; 4 g/10 (min)
Black carbon	2–2.5%

2.2 Uniaxial tensile tests UT

The uniaxial tensile tests UT were carried out on dumbbell specimens of type IV (Figure 2): thickness T = 6 mm, width of narrow section W_c = 6 mm, length of narrow section L = 33 mm, width overall W_o = 19 mm, length overall L_o = 100 mm, gage length G = 25 mm, distance between grips D = 65 mm, outer radius R_o = 25 mm, and radius of fillet R = 14 mm. The mechanical tests were carried out with a Zwick/Roell-type machine with a capacity of 20 kN [9].

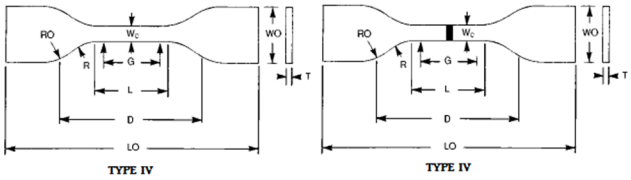

Figure 2: Specimens of uniaxial tensile test UT

All dimensions of the specimens are taken according to ASTM standard D638-03 [10]. The specimens were picked from the welded HDPE tube (butt-welding) parallel to the direction of extrusion and were stretched by two stretching speeds (V_e = 10 and 50 mm/min). For the two stretching rates proposed during the test, the true strain rate was determined graphically for each of the two cases studied.

3 Experimental results

The results obtained from the tensile tests for different stress velocities are shown in Figures 3–6. It is observed that the general appearance of stress–strain curves is characterized by four main zones: (I) a linear response that translates the elastic behavior to small deformations; a second part (II) which reflects the appearance of the plastic deformation; a third part (III) characterizing the beginning of the structural hardening stage because of the reorganization of the chains in the direction of stress; finally the last part (IV) marked by a hardening before the final rupture. These figures show that the mechanical behavior of these two different stretching speeds takes into account the sensitivity to the strain rate.

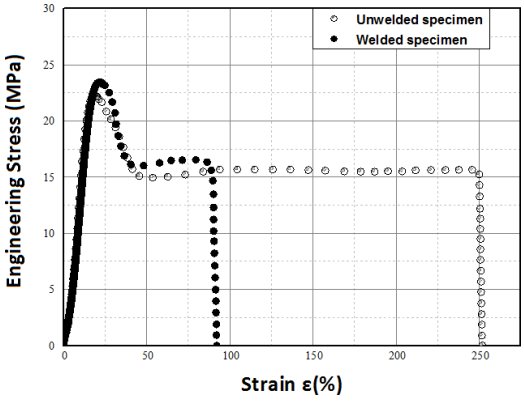

Figure 3: Stress–strain response of the uniaxial tensile tests (V_e = 10 mm/min)

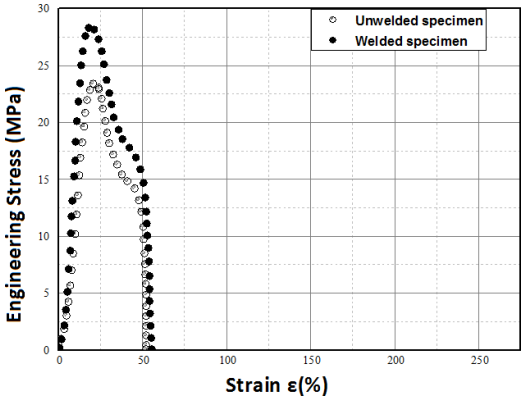

Figure 4: Stress–strain response of the uniaxial tensile tests (V_e = 50 mm/min)

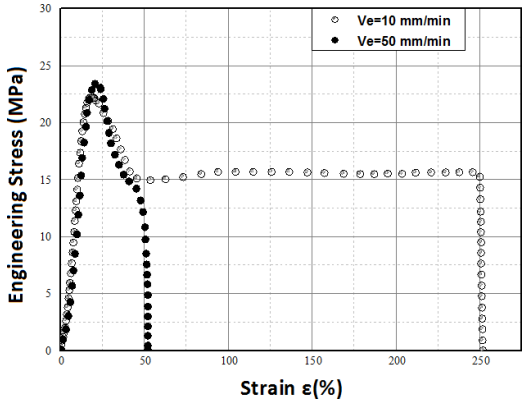

Figure 5: Stress–strain response of the uniaxial tensile tests for base material BM

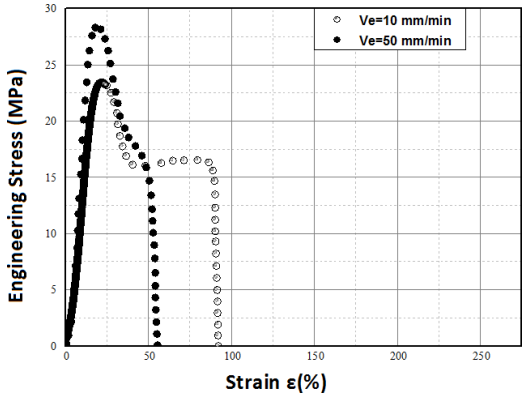

Figure 6: Stress–strain response of the uniaxial tensile tests for welded material

For the case of unwelded specimens, it is observed that the base material is ductile at high stress for which the lifetime is sensitive to the stress with a stressing speed V_e = 10 mm/min ($\dot{\epsilon}$ = 0.3 s^{-1}) and with an ultimate tensile strength of 249.899%. At a loading speed V_e = 50 mm/min ($\dot{\epsilon}$ = 1.6 s^{-1}), this material has a fragile character for which the lifetime is much less sensitive to stress because the strain at break is 46.82%. At the same loading speed V_e = 50 mm/min ($\dot{\epsilon}$ = 1.6 s^{-1}), this welded material has a fragile character for which the lifetime is much less sensitive to stress because the breaking strain is 44.51%. This means that the plastic deformation zone is larger in the case of the unwelded specimens than the welded ones.

From true stress–true strain curves (Figures 7–10) and in the case of the specimens made of base materials, it is observed that the studied HDPE presents a significant in-

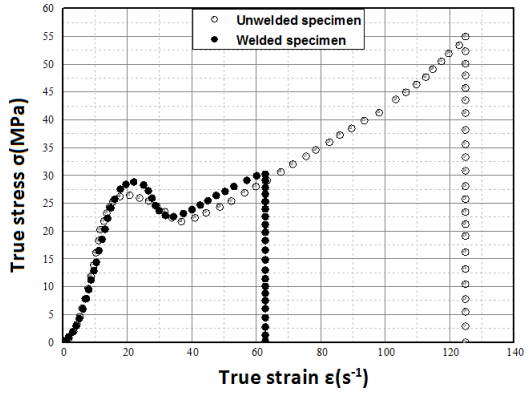

Figure 7: True stress–true strain curve of the uniaxial tensile tests for $\dot{\epsilon} = 0.3\ s^{-1}$

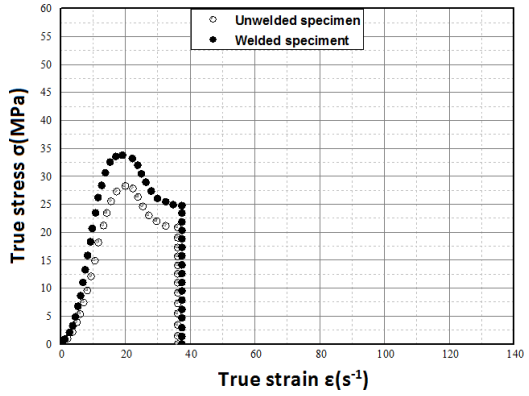

Figure 8: True stress–true strain curve of the uniaxial tensile tests for $\dot{\epsilon} = 1.6\ s^{-1}$

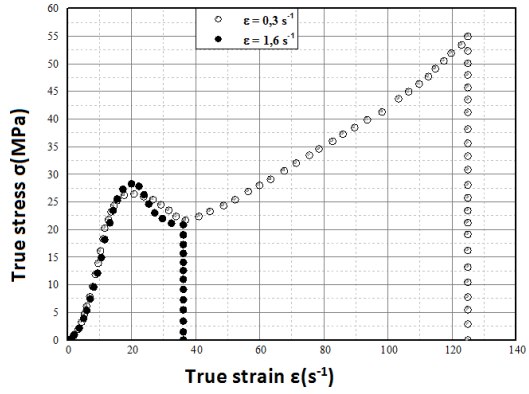

Figure 9: True stress–true strain curve of the uniaxial tensile tests for base material BM

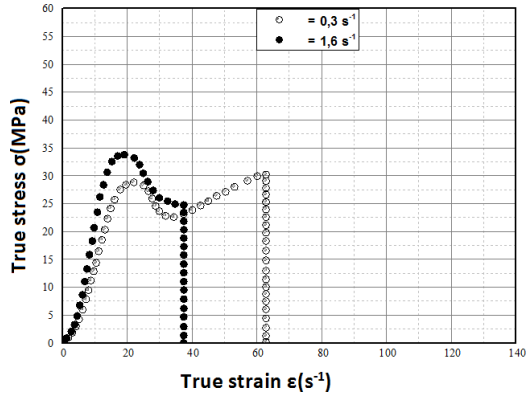

Figure 10: True stress–true strain curve of the uniaxial tensile tests for welded material

crease in the flow stress, with the rate of deformation depending on the Young's modulus. Some authors [11–13] have shown that this increase is because of the secondary process of the molecules. The HDPE exhibits a fragile behavior at different higher deformation rates. The true deformation rate has a great influence on the mechanical response of HDPE. In particular, the elastic limit increases with the rate of deformation.

At a low true deformation rate ($\dot{\epsilon} = 0.3\ s^{-1}$), and for both cases, specimens made of base material and welded material, the curves presented two parts: linear which can be interpreted as a linear elastic behavior which seems to have a true slope as a function of the deformation rate and the other nonlinear which indicates the sensitivity of the deformation velocity. On the other hand, by increasing the true strain rate ($\dot{\epsilon} = 1.6\ s^{-1}$), the curves do not reach the part that characterizes the curing stage before the final rupture. This leads us to say that welding with the proposed parameters at a true strain rate of $\dot{\epsilon} = 0.3\ s^{-1}$ is efficient.

4 Numerical study

The material studied may exhibit some hyperelastic behavior in addition to viscoelastic–viscoplastic performance. Numerically, using the calculation code for finite element used as models for both performances, it is sufficient to determine the related constants for the materials. The viscoelastic–viscoplastic constitutive model used in our study was developed as user-defined material and the material parameters were implemented in the UMAT to verify the constitutive equation.

The type of element used was C3D8R, which is an element with eight nodes of first order with reduced integration. The results of this simulation are related to the mesh of the specimen.

4.1 Constitutive models

In this work, three constitutive models are studied to characterize the material: elastic model, viscoelastic–viscoplastic model, and hyperplastic model.

4.1.1 Elastic model

It is well known that the criterion of plastic deformation can be expressed as follows::

$$f(\sigma_{ij}) = Y \tag{2}$$

The stress–strain relationship given in Equation (3) was adopted for plastic deformation, combined with a stress–strain polynomial relation in the elastic zone. This equation expresses the hardening part and was modified by Hutchinson and Neale [14].

To make calculations easier, the material used is considered to be isotropic. The relations are then reduced to those of Hooke's law of the theory of elasticity.

$$Y(\varepsilon) = \begin{Bmatrix} E\varepsilon \\ d\left[a(\varepsilon+b)^{(c-1)} - a(\varepsilon+b)^{-c}\right] + e \\ \alpha k \varepsilon^{N} \\ k\exp(M\varepsilon^{\beta}) \end{Bmatrix} \begin{matrix} (\varepsilon \le \varepsilon_y) \\ (\varepsilon_y \le \varepsilon \le \varepsilon_n) \\ (\varepsilon_n \le \varepsilon \le \varepsilon_t) \\ (\varepsilon \ge \varepsilon_t) \end{matrix} \tag{3}$$

4.1.2 Viscoelastic–viscoplastic model

The constitutive model used in the simulation was the combined viscoelastic–viscoplastic model implemented with the overlapping method.

Rheological models composed of springs and dashes are usually adopted in the modeling of the elastic–viscoplastic behavior of semicrystalline polymers [15] (Figure 11).

In general, rheology assumes that the physical properties of a polymer structure vary continuously from point to point. The rheology can be classified into three types:

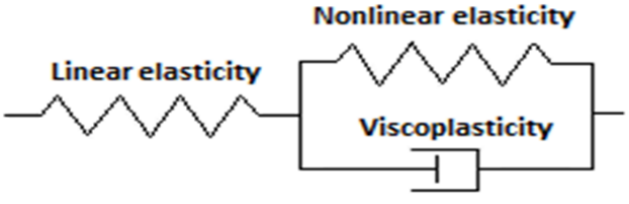

Figure 11: Rheology used to describe the wide range of deformation of vitreous polymers [17]

1. Experimental rheology: It determines experimentally the behavioral relationship between the stresses and the rate of deformation.
2. Structural rheology: It explains the behavior of the material from its structure.
3. Theoretical rheology: It provides mathematical models in a limited number of behaviors independently of the microscopic structure [16].

$$\left[C_{\alpha\beta}\right] = \begin{bmatrix} \lambda+2\mu & \lambda & \lambda & 0 & 0 & 0 \\ \lambda & \lambda+2\mu & \lambda & 0 & 0 & 0 \\ \lambda & \lambda & \lambda+2\mu & 0 & 0 & 0 \\ 0 & 0 & 0 & \mu & 0 & 0 \\ 0 & 0 & 0 & 0 & \mu & 0 \\ 0 & 0 & 0 & 0 & 0 & \mu \end{bmatrix} \tag{4}$$

$$\begin{bmatrix} \sigma_1 \\ \sigma_2 \\ \sigma_3 \\ \sigma_4 \\ \sigma_5 \\ \sigma_6 \end{bmatrix} = \frac{E}{(1+\nu)(2-\nu)} \tag{5}$$

$$\begin{bmatrix} 1-\nu & \nu & \nu & 0 & 0 & 0 \\ \nu & 1-\nu & \nu & 0 & 0 & 0 \\ \nu & \nu & 1-\nu & 0 & 0 & 0 \\ 0 & 0 & 0 & \frac{1}{2}(1-2\nu) & 0 & 0 \\ 0 & 0 & 0 & 0 & \frac{1}{2}(1-2\nu) & 0 \\ 0 & 0 & 0 & 0 & 0 & \frac{1}{2}(1-2\nu) \end{bmatrix}$$

$$\begin{bmatrix} \varepsilon_1 \\ \varepsilon_2 \\ \varepsilon_3 \\ \varepsilon_4 \\ \varepsilon_5 \\ \varepsilon_6 \end{bmatrix}$$

4.1.3 Hyperplastic model

Model Arruda–Boyce

The Arruda–Boyce model is based on molecular considerations to explain the mechanical behavior of stress–strain of polymer materials. This model calculates the deformation energy as the sum of the deformation energies of the individual chains [Equation (6)]:

$$W = \mu \sum_{i=0}^{5} \frac{c_i}{\lambda_m^{2i-2}} \times \left(i_1^i - 3^i\right) + \frac{1}{D}\left[\frac{J_{el}^2 - 1}{2} - Ln\left(J_{el}\right)\right] \tag{6}$$

where W is the deformation energy,
μ the shear modulus,

c constant material,
λ_m extended,
D the ratio of $2/k$,
k the low stress mass module,
J_{el} the elastic volume ratio,
and I the invariant of the strain tensor given by

$$I_1 = \lambda_1^2 + \lambda_2^2 + \lambda_3^2 \tag{7}$$

The deformation energy density function for the incompressible Arruda–Boyce model is given by [18]

$$W = Nk_B\theta\sqrt{n}[\beta\lambda_{chain} - \sqrt{n}Ln\left(\frac{\sinh\beta}{\beta}\right)] \tag{8}$$

Model Mooney–Rivlin

This model is an alternative to the phenomena of molecular models. The behavior of the polymers is only partially explained over the entire deformation spectrum.

For a given strain, the stress is determined as the derivatives of the strain energy density with respect to the deformation components.

Mooney and Rivlin then proposed a general expression of the free energy considered without a molecular interpretation of its terms. Mooney's main assumptions are that the polymer is incompressible and isotropic in its undeformed state. The Mooney–Rivlin model has as starting point the three deformation invariants (independent of the chosen coordinate system):

$$\begin{aligned} I_1 &= \lambda_1^2 + \lambda_2^2 + \lambda_3^2 \\ I_2 &= \lambda_1^2\lambda_2^2 + \lambda_2^2\lambda_3^2 + \lambda_3^2\lambda_1^2 \\ I_3 &= \lambda_1^2\lambda_2^2\lambda_3^2 \end{aligned} \tag{9}$$

where λ_1, λ_2, and λ_3 are three main extended reports.

The equation of the strain energy density is given by

$$W = C_{10}(I_{10} - 3) + C_{01}(I_2 - 3) \tag{10}$$

Model neo-Hookean

This model was established by the study of the polymer. The neo-Hookean model is a simplified model of the Mooney–Rivlin model. It is based on a reduced polynomial model when considering $N = 1$ n is introduced:

$$W = C_{10}(I_1 - 3) + \frac{1}{D_1}(J_{el} - 1)^2 \tag{11}$$

5 Numerical results

5.1 Characterization and law of mechanical behavior

The relations of the constitutive models (elastic and viscoelastic–viscoplastic) proposed were applied in the computation code/UMAT and compared with the experimental results of the uniaxial tension UT. The numerical results for the two deformation velocities ($\dot{\epsilon} = 0.3\ s^{-1}$) are shown in Figures 12–15. The numerical results for the two deformation rates ($\dot{\epsilon} = 0.3\ s^{-1}$ and $\dot{\epsilon} = 1.6\ s^{-1}$) are in very good agreement with the experimental results.

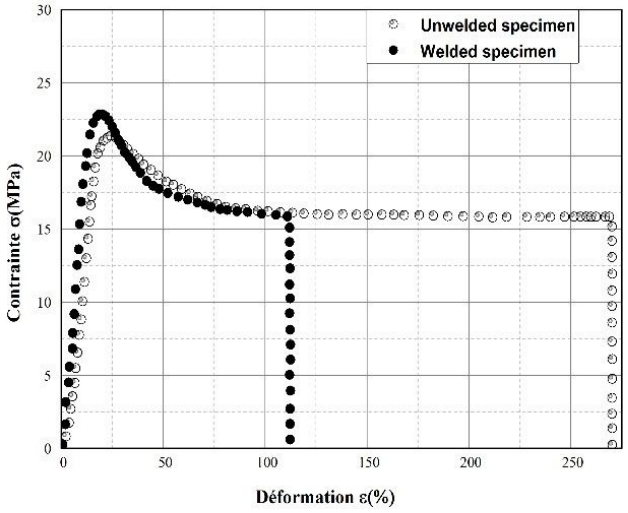

Figure 12: Stress–deformation curve obtained with the numerical simulation (V_e = 10 mm/min)

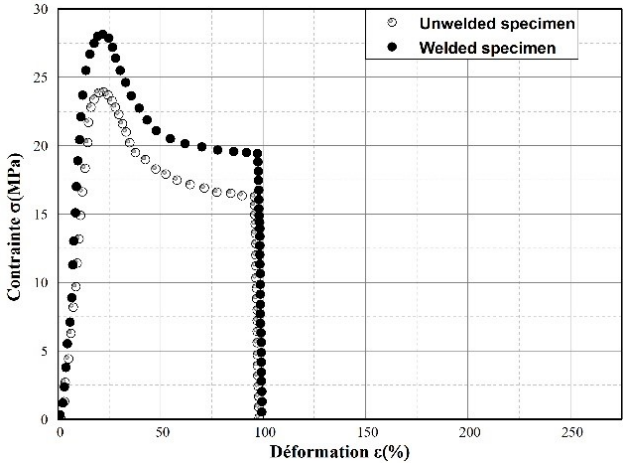

Figure 13: Stress–deformation curve obtained with the numerical simulation (V_e = 50 mm/min)

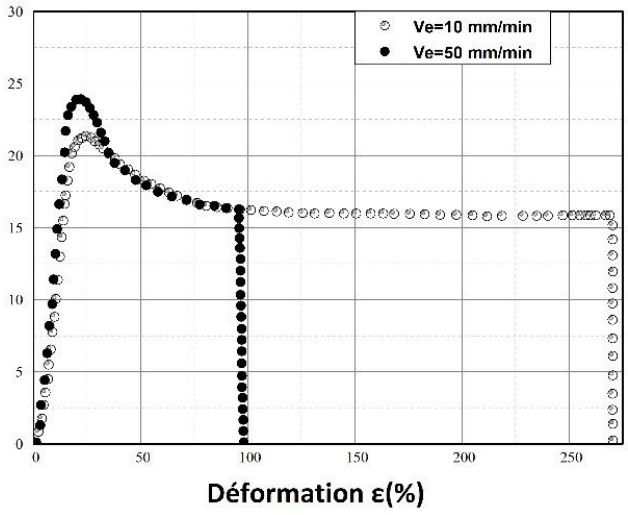

Figure 14: Stress–deformation curve obtained with the numerical simulation for base material BM

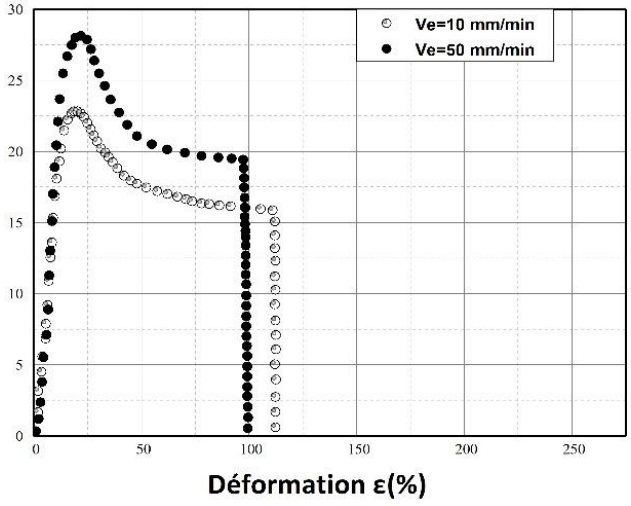

Figure 15: Stress–deformation curve obtained with the numerical simulation for welded material

5.2 Determination of the energy of deformations

In order to validate the experimental results of the tensile tests by numerical simulation, we carried out a second FEM simulation with available hyperelastic models to determine the deformation energy. The hyperelastic models were used (Arruda–Boyce, Mooney–Rivlin, neo-Hookean) by means of the theory of nonlinear elasticity. The main parameters of the hyperelastic models obtained in the simulation are summarized in Table 3.

Figures 16 and 17 illustrate the stress evolution as a function of the deformation of the hyperelastic models of base material. For the two applied stress rates ($\dot{\epsilon}$ = 0.3 and 1.6 s^{-1}), we observe that the neo-Hookean model gives the same pace as the Mooney–Rivlin model.

Table 3: Main Parameters of Hyperelastic Models

Models	ϵ' (s^{-1})	Parameters	
		MB	Soudée
Arruda–Boyce	0.3	μ = 9.1315 E–04	μ = 14.0510434
		λ_m = 378826.204	λ_m = 2213.48407
	1.6	μ = 17.7559506	μ = 15.5155384
		λ_m = 1922.25720	λ_m = 1563.50034
Mooney–Rivlin	0.3	C_{10} = 2.671236 E–04	C_{10} = –-17.4803690
		C_{01} = 3.027694 E–02	C_{01} = 39.8352694
	1.6	C_{10} = –45.0613426	C_{10} = –64.0309077
		C_{01} = 75.5391736	C_{01} = 104.608040
Neo-Hookean	0.3	C_{10} = 2.671236 E–04	C_{10} = 7.02552245
		C_{01} = 3.027694 E–02	
	1.6	C_{10} = 8.87797635	C_{10} = 7.75777069

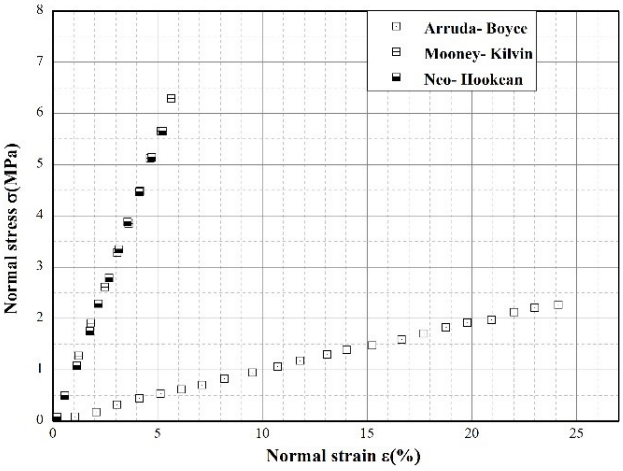

Figure 16: Stress–strain curve of hyperplastic models for base material BM ($\dot{\epsilon}$ = 0.3 s^{-1})

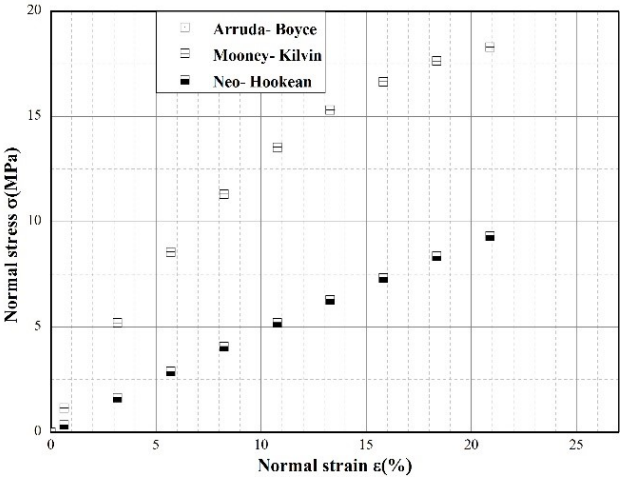

Figure 17: Stress–strain curve of hyperplastic models for base material BM ($\dot{\epsilon}$ = 1.6 s^{-1})

For the case of the welded specimens, Figures 18 and 19 give different results of the two models (neo-Hookean and Mooney–Rivlin) and this means that there is an influence of the welding parameters on the deformation energy.

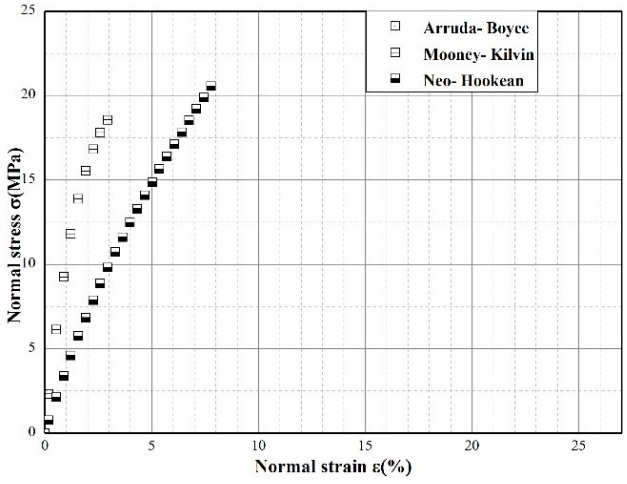

Figure 18: Stress–strain curve of hyperplastic model for welded specimens ($\dot{\epsilon}$ = 0.3 s^{-1})

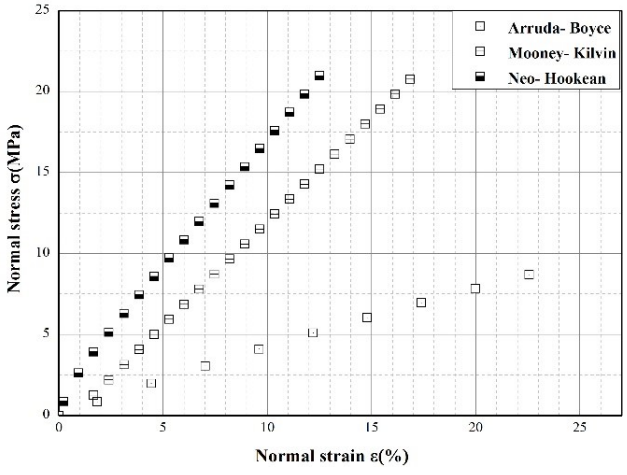

Figure 19: Stress–strain curve of hyperplastic model for welded specimens ($\dot{\epsilon}$ = 1.6 s^{-1})

6 Conclusion

In this work, the influence of stretching speed (V_e) and strain rate ($\dot{\epsilon}$) on the behavior of the welded tube is studied at the proposed conditions. The welded tube is a widely used material in industrial field, namely HDPE.

We carried out an experimental study to test the sensitivity of both unwelded and welded structures by the butt-welding technique. The results of our research agree with the mechanical behavior of many polymers. For the two studied cases, the behavior of the HDPE used is relatively well known at the high stretching speed (V_e = 50 mm/min) and the high strain rate ($\dot{\epsilon}$ = 1.6 s^{-1}). In the case of welded specimens and after testing, the results showed the effect of the fused part (welding bead) on the overall behavior. It is observed that this fused part does not maintain the same mechanical characteristics despite the use of the same welding parameters.

Two comparisons were made between the experimental and numerical results:

1. Results of the tensile tests of the base material
2. Results of the tensile tests of the welded material

The comparison between the experimental and numerical results of base material BM subjected to the tensile loads (V_e = 10 and 50 mm/min) shows a good correlation between the numerical model (viscoelastic–viscoplastic) and the experimental results obtained. It is thus concluded that the model used is applicable for HDPE.

The results of the tensile tests carried out at different stress speeds (welded material) were also compared. It is summarized that the drawing speed of the welded specimens caused an increase in the elastic limit and reduced the breaking strength. Unwelded specimens indicate a higher yield strength than welded specimens at all stretch speeds.

References

[1] Costa, A. P. D., Botelho, E. C., Costa, M. L., Narita, N. E. and Tarpani, J. R.: A Review of Welding Technologies for Thermoplastic Composites in Aerospace Applications. Aerosp. Technol. Manag. São José dos Campos, 4(3), 255-265, 2012.

[2] Neale, K. W. and Tugcu, P.: Analysis of necking and neck propagation in polymeric materials. Journal of the Mechanics and Physics of Solids, 33(4), 323–337, 1985.

[3] Zhang, P.Y. Yi. and Jar, B.: Phenomenological modelling of tensile fracture in PE pipe by considering damage evolution. Materials and Design, 77, 72–82, 2015.

[4] Butler, M. F., Donald, A. M.: Deformation of spherulitic polyethylene thin film. J. Mater. Sci, 32, 3675-3685, 1997.

[5] Butler, M. F., Donald, A. M. and Ryan, A. J.: Time resolved simultaneous small and wide-angle X-ray scattering during polyethylene deformation-II. Cold drawing of linear polyethylene. Polym, l(39), 39-52,1998.

[6] Aboulfaraj, M., G'sell, C., Ulrich, B., Dahoun, A.: In situ observation of plastic deformation of polypropylene spherulites under uniaxial tension and simple shear in the scanning electron microscope. Polym, 36, 731-742, 1995.

[7] Butler, M. F., Donald, A. M.: Deformation of spherulitic polyethylene thin film. J. Mater. Sci, 32, 3675-3685, 1997.

[8] Djebli, A., Aid, A., Bendouba, M., Talha, A., Benseddiq, N., Benguediab, M., Zengah, S.: Uniaxial Fatigue of HDPE-100 Pipe. Engineering, Technology & Applied Science Research, 4(2), 600-604, 2004.

[9] Laboratoire Mécanique et Physique des matériaux. Université Djillali Liabes. Sidi Bel Abbès. Algérie.

[10] ASTM D638.: Standard Test Method for Tensile Properties of Plastics. part IIB Plastics (I), l. 8(1), 1-15, 2003.

[11] Rietsch, F., Bouette, B.: The compression yield behaviour of polycarbonate over a wide range of strain rates and temperatures. European Polymer Journal, (26), 1071-1075, 1990.

[12] Richeton, J., Ahzi, S., Daridon, L., Rémond, Y.: A formulation of the cooperative model for the yield stress of amorphous polymers for a wide range of strain rates and temperatures. Polymer, (46), 6035-6043, 2005.

[13] Richeton, J., Ahzi, S., Vecchio, K. S., Jiang, F. C., Adharapurapu, R. R.: Influence of temperature and strain rate on the mechanical behavior of three amorphous polymers: Characterization and modelling of the compressive yield stress. International Journal of Solids and Structures, (43), 2318-2335, 2006.

[14] Hutchinson, J. W., Neale, K. W.: Neck propagation. Journal of the Mechanics and Physics of Solids, 31(5), 405–426, 1983.

[15] Clausen, A. H., Loria, M. P., Berstad, T. and Hopperstad, O. S.: A constitutive model for thermoplastics With some applications. 8th European LS-DYNA Users Conference, Strasbourg - May 2011.

[16] Neale, K. W., Tugcu, P.: Analysis of necking and neck propagation in polymeric materials. Journal of the Mechanics and Physics of Solids, 33(4), 323–337, 1985.

[17] Arruda, E. M., Boyce, M. C.: Evolution of plastic anisotropy in amorphous polymers during finite straining. International Journal of Plasticity, 9(6), 697–720, 1993.

[18] Bergstrom, J. S. and Boyce, M. C.: Deformation of Elastomeric Networks: Relation between Molecular Level Deformation and Classical Statistical Mechanics Models of Rubber Elasticity. Macromolecules, 34(3), 614–626, 2001.